Atomic structure of amorphous $Al_{100-2x}Co_xCe_x$ ($x=8$, 9, and 10) and $Al_{80}Fe_{10}Ce_{10}$ alloys: An XAFS study

A. N. Mansour,* C.-P. Wong, and R. A. Brizzolara
Naval Surface Warfare Center, Weapons Research and Technology Department, 10901 New Hampshire Avenue, Silver Spring, Maryland 20903-5000
(Received 19 April 1994)

The local atomic structure of Co, Fe, and Ce in aluminum-rich amorphous alloys of $Al_{100-2x}Co_xCe_x$ ($x=8$, 9, and 10) and Ce in $Al_{80}Fe_{10}Ce_{10}$ has been investigated by x-ray-absorption fine structure (XAFS) spectroscopy. The materials, 1- and 3-μm-thick films, were prepared by vapor quenching using the dc magnetron sputtering method. We show that the composition of the glass-forming region of these magnetron-sputtered alloys strictly follows the theoretical limit calculated on the basis of the atomic size criterion. From analyses of the XAFS data at the K edges of Co and Fe and the L_3 edge of Ce, the following conclusions with regard to local structure are made. The first coordination sphere of Co in $Al_{100-2x}Co_xCe_x$ ($x=8$, 9, and 10) consists of 5.8 to 6.4 Al atoms at a distance of 2.44 Å. The local coordination sphere for Fe in $Al_{80}Fe_{10}Ce_{10}$ consists of 6.4 Al atoms at a distance of 2.47 Å. Ce in both systems appears to be coordinated with roughly 5 and 9 Al atoms at distances of 2.95 and 3.15 Å, respectively. These results are discussed in light of the dense random packing (DRP) of hard spheres model. Both Co-Al and Fe-Al bond lengths are anomalously short (9 and 8 % contraction, respectively) with also anomalously low coordination numbers (45% reduction) from values based on the DRP model using the metallic state radii. These anomalous changes indicate a strong interaction between Co or Fe atoms and the Al atoms which perhaps may be a result of a covalently bonded environment. The Ce-Al distance in both the Al-Co-Ce and Al-Fe-Ce systems, on the other hand is smaller by only 0.17 Å (a contraction of only 5%) and the coordination number is reduced by only 13% from expected values based on the DRP model. The contraction in the distance and reduction in the coordination number for Ce are much smaller than those values of the Co or Fe and, hence, the local bonding for Ce is likely to be metallic in character.

INTRODUCTION

Aluminum-based metallic glasses with remarkably high Al content are relatively new materials that were discovered independently by He, Poon, and Shiflet,[1] and Tsai, Inoue, and Masumoto.[2] Typical composition is Al-TM-R where TM is a late transition element such as iron, cobalt, or nickel and R is yttrium or a rare-earth element such as gadolinium or cerium. These amorphous alloys can be prepared with extremely high aluminum content either by vapor quenching using the dc magnetron-sputtering method[3] or rapid solidification from the liquid phase using the melt-spinning method.[1,2] The amorphous phase is formed with an Al content as high as 84 at. % for samples prepared by the magnetron-sputtering process and as high as 90 at. % for samples prepared by the melt-spinning process. These materials are truly noncrystalline alloys which combine the properties of a metal with the short-range order of a glass. They are very homogeneous and lack the defects such as grain boundaries and dislocations typical of a crystalline material. The homogeneity and the lack of grain boundaries have led to a number of remarkable mechanical[4,5] and magnetic[6] properties.

Several factors referred to as "the alloy-chemical factors" are known to be correlated with the ease of glass formation. These include the atomic sizes of various elements composing the alloy, valence electron concentration, and the heat of compound formation.[7] Among these factors, the atomic sizes are of relevance to the present investigation. It is known that the glass-forming region of melt-spun Fe-based systems extends outside the theoretical limit based on the nominal atomic sizes. Recent neutron and x-ray structural studies[8,9] of melt-spun $Al_{90}Fe_7Ce_3$ and $Al_{90}Fe_5Ce_5$ alloys revealed a strong interaction in the vicinity of the first coordination sphere of Fe. This interaction is characterized by an anomalously short distance and low coordination number compared to values derived on the basis of the dense random packing of hard spheres model. In these studies, it was argued that the strong interaction is associated with charge transfer from the Al to the Fe atoms.

A fundamental understanding of the effects of preparation methods and composition on the ease of glass formability through determination of the local atomic structure is necessary so that preparation conditions can be tailored to produce alloys with high stability. In this paper, we report on the local atomic structure in the vicinity of Co, Fe, and Ce in magnetron-sputtered $Al_{100-2x}Co_xCe_x$ ($x=8$, 9, and 10) and $Al_{80}Fe_{10}Ce_{10}$ amorphous alloys as determined by x-ray-absorption fine structure (XAFS) spectroscopy from analysis of both the x-ray-absorption near-edge structure (XANES) and the extended x-ray-absorption fine structure (EXAFS). We will show that the glass-forming region of magnetron sputtered AL-Co(Fe)-Ce material strictly follows the

theoretical limits derived on the basis of the atomic size criterion.

EXPERIMENT

Sample preparation

Two sets of samples were prepared. In the first set, four 1-μm-thick coatings of $Al_{100-2x}Co_xCe_x$ ($x=7$, 8, 9, and 10) were deposited on glass slides. In the other set, two samples of 3-μm-thick coatings of $Al_{80}Co_{10}Ce_{10}$ and $Al_{80}Fe_{10}Ce_{10}$ were deposited directly on the adhesive side of Kapton tape. Deposition of films was made by vapor quenching using the dc magnetron-sputtering method. Substrates were mounted on a simultaneously rotating and revolving fixture to ensure uniformity of film thickness and composition. During deposition of the films, the substrates were kept at ambient temperature. Commercial sputtering targets, fabricated from 3N pure metals with composition $Al_{80}Fe_{10}Ce_{10}$ and $Al_{80}Co_{10}Ce_{10}$, were obtained from Sputtered Films, Inc., Santa Barbara, California. The films with compositions $Al_{80}Fe_{10}Ce_{10}$ and $Al_{80}Co_{10}Ce_{10}$ were deposited from the commercial targets of $Al_{80}Fe_{10}Ce_{10}$ and $Al_{80}Co_{10}Ce_{10}$, respectively, by sputtering at an operating power of 400 W. Deposition of the $Al_{82}Co_9Ce_9$ and $Al_{84}Co_8Ce_8$ films was achieved by cosputtering from a pure Al and $Al_{80}Co_{10}Ce_{10}$ targets at an operating power of 400 W for the alloy and 100 and 200 W, respectively, for the pure metal. Deposition rate is estimated to be 170 Å per minute. At this rate sputtering for 1 and 3 h was necessary for manufacturing 1- and 3-μm-thick films, respectively. Atomic concentrations and film thicknesses were determined using atomic absorption spectroscopy and Rutherford backscattering methods as described by Kabacoff *et al.*[3]

XRD and XAFS measurements

The x-ray-diffraction measurements were collected using monochromatized Cu $K\alpha$ x rays on a Siemens (model: Diffrac 500) unit. The x-ray-absorption experiments were performed on beamline X-11A of the National Synchrotron Light Source (NSLS) at Brookhaven National Laboratory with the electron storage ring operating at an electron energy of 2.5 GeV and a stored current in the range of 110 to 220 mA.[10] Data were collected with a variable exit double-crystal monochromator using two flat Si(111) crystals. Harmonics were rejected by detuning the parallelism of the monochromator crystals. This is achieved by a piezoelectric transducer to adjust the top crystal until the harmonic content is minimized. Spectra of the Ce L_3-edge and Co K-edge data for the first set of samples (1-μm-thick coatings on glass slides) were obtained using the fluorescence yield detection mode.[11] The films were pulled from the glass slide with the aid of Kapton tape and then stacks of 12 and 24 layers for each sample were sandwiched and used to make these measurements. Spectra for the Ce L_3 edge, Co K edge, and Fe K edge for the second set of samples (3-μm-thick coatings on Kapton tape) were obtained using the transmission detection mode. In these measurements 12 and 10 layers of 3-μm-thick $Al_{80}Co_{10}Ce_{10}$ and $Al_{80}Fe_{10}Ce_{10}$ films, respectively, were stacked together giving a Co K-edge jump ($\Delta\mu x$) of 0.37 and an Fe K-edge jump ($\Delta\mu x$) of 0.38. For the Ce L_3-edge measurements, on the other hand, four and nine layers of 3-μm-thick $Al_{80}Cu_{10}Ce_{10}$ and $Al_{80}Fe_{10}Ce_{10}$ films were stacked giving a $\Delta\mu x$ of 0.43 and 0.86, respectively. The fluorescence data was obtained using a specialized fluorescence ion chamber detector.[12] The x-ray intensities were monitored using ionization chambers filled with nitrogen gas for the incident beam, an appropriate mixture of nitrogen and argon gases for the transmitted beam, and Krypton gas for fluorescence signal. The background component due to elastic and Compton scattering of the incident x rays was minimized by using an aluminum Soller slit assembly and V, Mn, and Fe filters, each with an effective thickness of three absorption lengths, for the Ce L_3 edge, Fe K edge, and Co K edge, respectively. The energy calibration for Co, Fe, and Ce was monitored using a Co foil, a Fe foil, and a CeO_2 reference materials and employing a third ion chamber filled with the same gas as that of the transmitted beam ion chamber.

Reference samples of bulk Co (5-μm-thick foil), bulk Fe (5-μm-thick foil), Fe_2O_3, $Ce(NO_3)_3$, and CeO_2 were also investigated to serve as standards for comparison purposes and subsequent data analysis. The XAFS measurements for both foils, Fe_2O_3, $Ce(NO_3)_3$, and CeO_2 were made in the transmission mode. Research grade high-purity powders of Fe_2O_3, $Ce(NO_3)_3$, and CeO_2 were prepared for the x-ray-absorption measurements by grinding into a fine powder and selecting small particles less than 20 μm in size by sieving through a 20-μm-size nylon screen. The fine powder was then deposited on Kapton tape and several layers were then stacked to give a relatively uniform thickness appropriate for XAFS measurements made in the transmission mode. Two and four layers were used in separate runs for Fe_2O_3 giving a $\Delta\mu x$ of 0.53 and 1.00, respectively. Six layers were used for $Ce(NO_3)_3$ giving a $\Delta\mu x$ of 0.64. Two and four layers were used for CeO_2 giving a $\Delta\mu x$ of 0.26 and 0.60, respectively. All spectra presented here were measured at room temperature (300 K).

RESULTS

Based on both experimental data and theoretical treatments of topological atomic stresses,[7,13] it was demonstrated that the composition of the glass-forming region can be estimated from the atomic size factor, λ, given by

$$\lambda = C_B\left|1-\left[\frac{R_B}{R_A}\right]^3\right| + C_C\left|1-\left[\frac{R_C}{R_A}\right]^3\right|, \qquad (1)$$

where C is the concentration in atomic percent and R is the atomic radius. The subscripts A, B, C refer to the matrix (i.e., Al) and solute components Co (or Fe) and Ce, respectively. Using nominal atomic radii (metallic state) of $R_{Al}=1.43$, $R_{Co}=1.25$, $R_{Fe}=1.26$, and $R_{Ce}=1.82$ Å, the atomic size factors for the various alloys examined in this investigation were determined and are listed in Table I. The minimum solute concentration

TABLE I. Summary of atomic size factor as a function of composition.

Composition	λ (using metallic state radii)	λ (using amorphous state radii)
$Al_{80}Co_{10}Ce_{10}$	0.139	0.126
$Al_{82}Co_9Ce_9$	0.125	0.113
$Al_{84}Co_8Ce_8$	0.112	0.100
$Al_{86}Co_7Ce_7$	0.098	0.087
$Al_{80}Fe_{10}Ce_{10}$	0.141	0.126

required to form an amorphous phase is given by the criterion

$$\lambda \simeq 0.1 \ . \tag{2}$$

In this case, where equal concentrations of the solute components are used, the minimum solute concentrations required to form an amorphous phase are $C_{Fe}=C_{Ce}=7.1$ for the Al-Fe-Ce and $C_{Co}=C_{Ce}=7.2$ for the Al-Co-Ce systems. This is confirmed in Fig. 1 which shows a comparison of the x-ray-diffraction patterns for $Al_{82}Co_9Ce_9$ and $Al_{86}Co_7Ce_7$. The x-ray-diffraction pattern for the $Al_{82}Co_9Ce_9$ displays two amorphous bands. One band, in the 2θ range of 6°–30°, originates from the glass slide substrate. The second band, in the 2θ range of roughly 30°–50°, originates from the film of the amorphous alloy. The x-ray-diffraction pattern of $Al_{86}Co_7Ce_7$, on the other hand, displays sharp peaks characteristic of a crystalline phase, in addition, to the amorphous bands. The composition and crystal structure of the crystalline phase are unknown at the present time. The x-ray-diffraction patterns for $Al_{80}Co_{10}Ce_{10}$ and $Al_{84}Co_8Ce_8$ are similar to that of $Al_{82}Co_9Ce_9$ and none consisted of sharp peaks characteristic of crystalline phases. The x-ray-diffraction patterns for the Fe system are similar to those of the Co system and will not be discussed here.

Now, we turn our attention to the XAFS data. The experimentally measured x-ray-absorption cross section $\mu_0(E)x$, where E is the x-ray photon energy and x is the sample thickness, is given by $\ln(I_0/I)$ for transmission data and I_f/I_0 for fluorescence data where I_0, I, and I_f are the incident, transmitted, and fluorescence yield intensities, respectively. In determining $\mu_0 x$ from fluorescence yield measurements, correction for the energy dependence of the gas absorption cross section for the incident x-ray intensity was made using cross sections calculated with McMaster coefficients.[14] The pre-edge background absorption, $\mu_p(E)x$, was determined from a quadratic fit to the data roughly 300–30 eV below the edge energy and then extrapolating over the entire energy range of the spectrum. The K-edge absorption, $\mu(E)x$, was then isolated by subtracting $\mu_p(E)x$ from $\mu_0(E)x$. The smoothly varying atomic absorption, $\mu_a(E)x$, was determined by fitting the post edge data of $\mu(E)x$ with a cubic spline function.[15,16] An energy-independent step normalization was then applied by dividing $\mu(E)x$ with the value of the atomic absorption, $\mu_a(E_n)x$, where E_n is the normalization energy and was taken to be 100 eV above the edge energy.

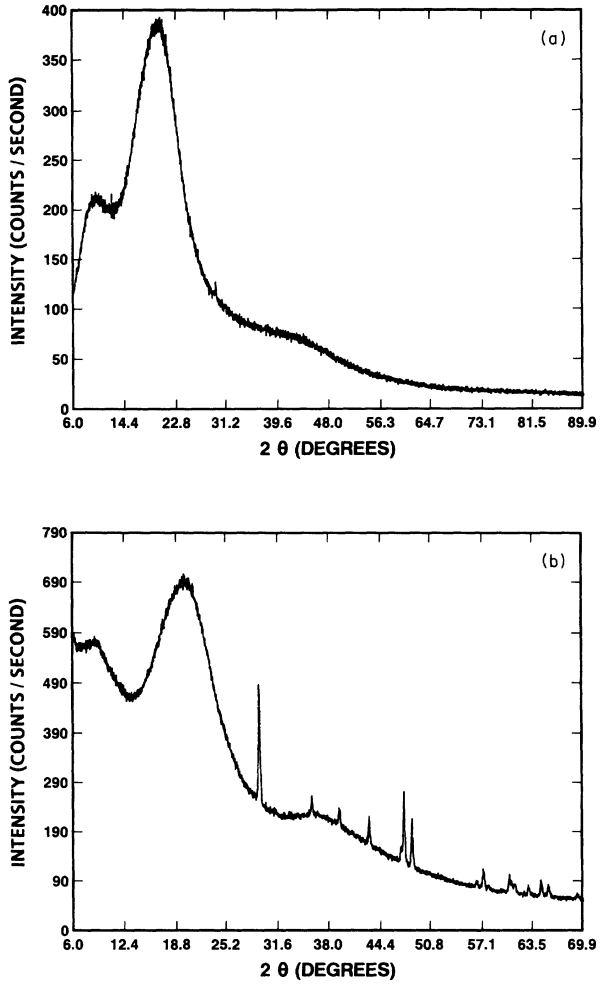

FIG. 1. (a) X-ray-diffraction pattern for 1-μm-thick film of $Al_{82}Co_9Ce_9$ showing two amorphous bands arising from the glass slide (2θ range of 6°–30°) and the film of the amorphous alloy (2θ range of 30°–50°). (b) X-ray-diffraction pattern for 1-μm-thick film of $Al_{86}Co_7Ce_7$ showing sharp diffraction peaks arising from a crystalline phase (whose identity and structure unknown at the present time) in addition to the two amorphous bands observed in (a).

Next, the extended x-ray-absorption fine structure (EXAFS) region of the XAFS spectrum, $\chi(k)$, was extracted and normalized according to

$$\chi(k)=\left[\frac{\mu(k)-\mu_a(k)}{\mu_a(k_n)}\right]\left[\frac{\mu_m(k_n)}{\mu_m(k)}\right], \tag{3}$$

where k is the photoelectron wave number defined according to

$$k=\sqrt{(8\pi^2 m/h^2)(E-E_0)} \tag{4}$$

with m being the electron mass, h is Planck's constant, E_0 is set equal to 7711.0, 7112.0, and 5721.0 eV corresponding to the Co K-edge, Fe K-edge, and Ce L_3-edge data, respectively, and $\mu(k)$ and $\mu_a(k)$ are as described

previously. The term $\mu_m(k)$ is the atomic absorption calculated with McMaster coefficients[14] which provides the energy-dependent McMaster normalization and k_n is the photoelectron wave number corresponding to the normalization energy E_n. The energy-dependent normalization is necessary if one chooses to use *ab initio* theoretical backscattering amplitude and phase values such as those calculated with the FEFF code[17,18] to extract the structural parameters, as is the case in the present analysis.

The normalized x-ray-absorption near-edge structure (XANES) of Co K edge and Fe K edge for the 3-μm-thick films of $Al_{80}Co_{10}Ce_{10}$ and $Al_{80}Fe_{10}Ce_{10}$ are shown in Figs. 2 and 3, respectively. These spectra are being compared with the XANES spectra of structurally well known polycrystalline Co and Fe foils. The spectra display the normalized K-edge absorption, μx, as a function of photon energy. As mentioned previously, the XAFS spectra for each sample and its respective calibration foil were measured simultaneously to ensure accurate alignment of both edges with respect to each other. Visual examination of spectra in Figs. 2 and 3 reveals that at the onset of the edge the data for both alloys are shifted to lower energies relative to the edge data of their respective comparison standards. This shift can be interpreted to indicate an increase in the electron density around both Co and Fe in the alloy samples due to a charge transfer of electrons from neighboring Al atoms of the first coordination sphere. It will be shown later in the text that the first coordination sphere for both Co and Fe consists exclusively of Al atoms.

The normalized Co K-edge EXAFS data, $k^3\chi(k)$, of the 1-μm-thick films of $Al_{80}Co_{10}Ce_{10}$ and $Al_{84}Co_8Ce_8$ taken in the fluorescence mode are shown in Fig. 4. Aside from an amplitude variation, the data for both samples are very similar. The frequencies of the EXAFS oscillations for both samples match each other very closely.

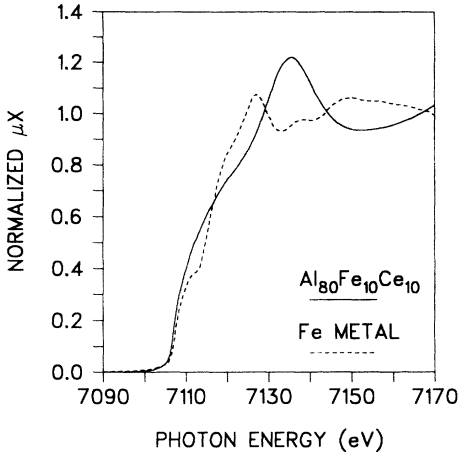

FIG. 3. Comparison of normalized Fe K-edge XANES data for a 3-μm-thick film of $Al_{80}Fe_{10}Ce_{10}$ and Fe foil showing that the data at the onset of the edge for the alloy is shifted to lower energies relative to that of the foil indicating a charge transfer from the Al atoms of the first coordination sphere to Fe.

The $k^3\chi(k)$ spectrum for the $Al_{82}Co_9Ce_9$ sample (not shown) is similar to those displayed in Fig. 4 except for an amplitude that is intermediate between those for the $Al_{80}Co_{10}Ce_{10}$ and $Al_{84}Co_8Ce_8$. A comparison of the phase uncorrected Fourier transforms of the Co K-edge EXAFS spectra displayed in Fig. 4 is shown in Fig. 5. Each spectrum displays mainly a single peak arising from the first coordination sphere and no prominent structure from higher coordination spheres. The absence of peaks from higher coordination spheres is indicative of the amorphous nature of these alloys. A comparison of the local structure from the first coordination sphere for the three $Al_{100-2x}Co_xCe_x$ ($x=8,9,10$) on an expanded scale

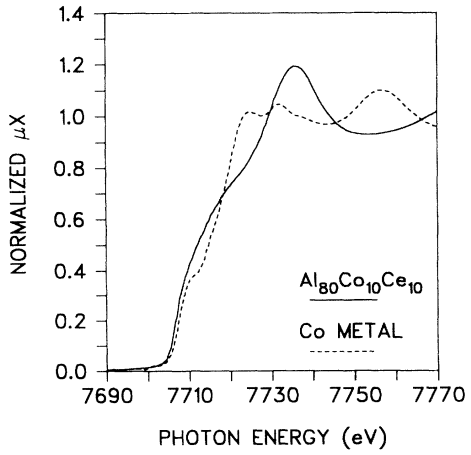

FIG. 2. Comparison of normalized Co K-edge XANES data for 1-μm-thick film of $Al_{80}Co_{10}Ce_{10}$ and Co foil showing that the data at the onset of the edge for the alloy is shifted to lower energies relative to that of the foil indicating a charge transfer from the Al atoms of the first coordination sphere to Co.

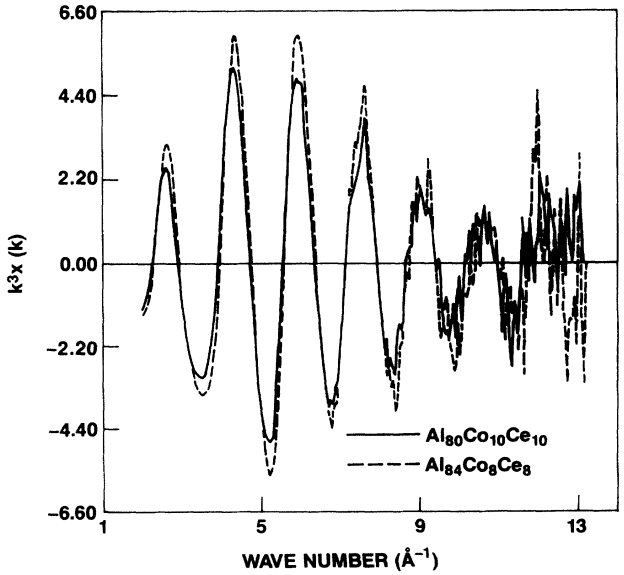

FIG. 4. Comparison of normalized Co K-edge EXAFS data, $k^3\chi(k)$, for $Al_{80}Co_{10}Ce_{10}$ and $Al_{84}Co_8Ce_8$.

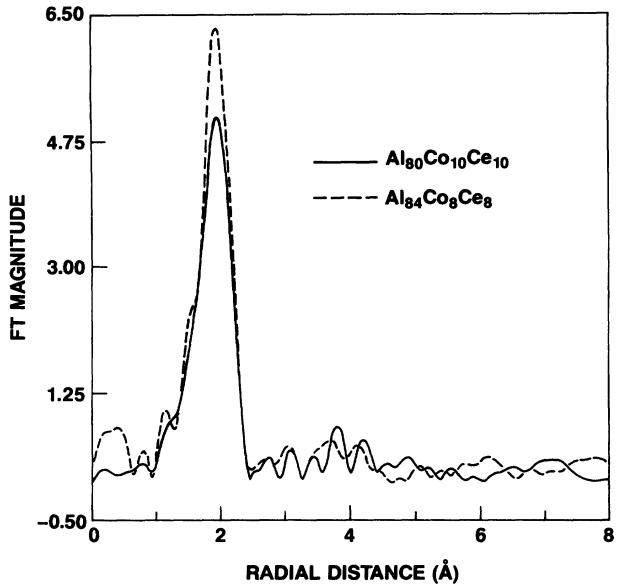

FIG. 5. Comparison of Fourier transform of normalized Co K-edge EXAFS data, $k^3\chi(k)$, for 1-μm-thick films of $Al_{80}Co_{10}Ce_{10}$ and $Al_{84}Co_8Ce_8$ (Δk: 2.25–11.8 Å^{-1}).

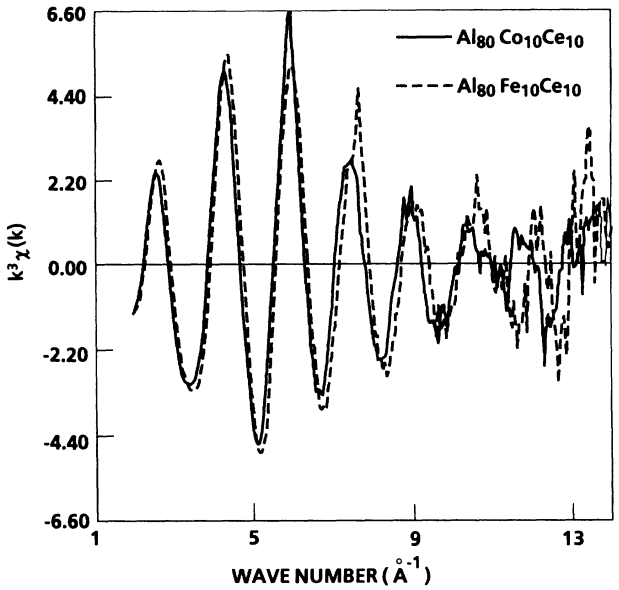

FIG. 7. Comparison of normalized Co and Fe K-edge EXAFS data, $k^3\chi(k)$, for 3-μm-thick films of $Al_{80}Co_{10}Ce_{10}$ and $Al_{80}Fe_{10}Ce_{10}$.

is shown in Fig. 6. It indicates that the peak position is independent of composition. The only difference is in the amplitude of the Fourier transform peak which increases with increase in Al content or increase in the Al/Co atomic percent ratio. The increase in the amplitude of the Fourier transform peak with increase in Al content may be due to an increase in the coordination number and/or a decrease in the disorder of the first coordination sphere which will be further discussed later in the text.

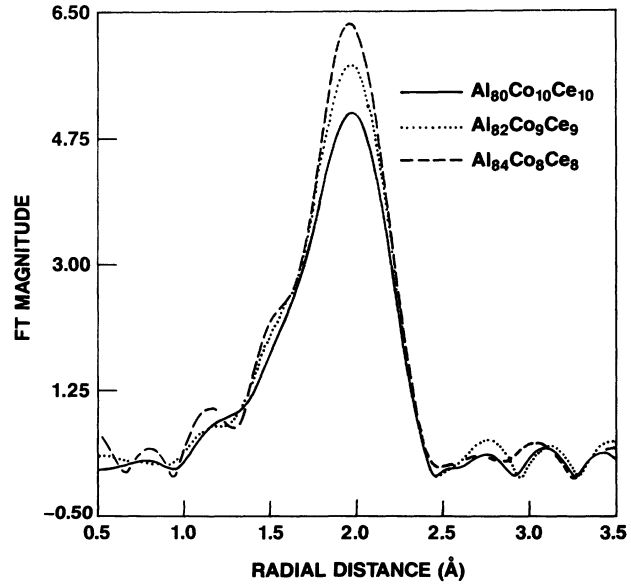

FIG. 6. Comparison of Fourier transforms of normalized Co K-edge EXAFS data, $k^3\chi(k)$, on an expanded scale of 1-μm-thick films for $Al_{80}Co_{10}Ce_{10}$, $Al_{82}Co_9Ce_9$, and $Al_{84}Co_8Ce_8$ (Δk: 2.25–11.8 Å^{-1}).

A comparison of the normalized Co and Fe K-edge EXAFS spectra, $k^3\chi(k)$, for the 3-μm-thick films of $Al_{80}Co_{10}Ce_{10}$ and $Al_{80}Fe_{10}Ce_{10}$ taken in the transmission mode is shown in Fig. 7. A slight mismatch in the frequency of the data at high k values is observed due to a smaller Co-Al bond length compared to the Fe-Al bond length (as will be shown later in the text). Fourier transforms of spectra in Fig. 7 are displayed in Fig. 8. Examination of the data in both figures reveals that the local structure of Co is qualitatively similar to that of Fe. The greater amplitude for the first peak in the Fourier trans-

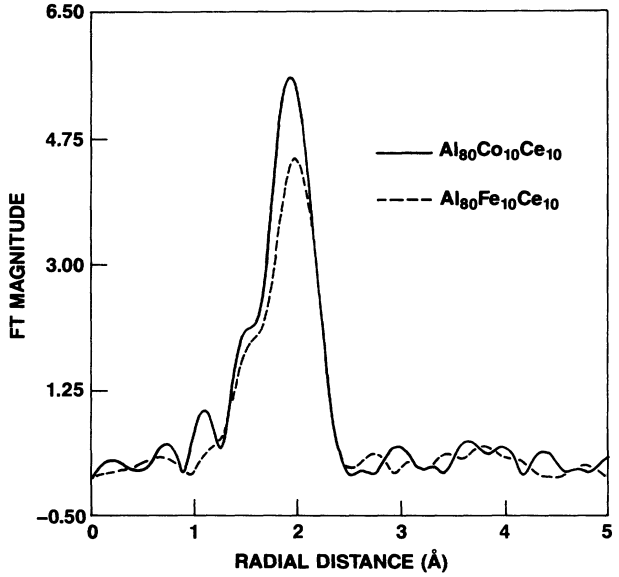

FIG. 8. Comparison of Fourier transforms of normalized Co and Fe K-edge EXAFS data, $k^3\chi(k)$, for 3-μm-thick films of $Al_{80}Co_{10}Ce_{10}$ and $Al_{80}Fe_{10}Ce_{10}$ (Δk: 2.20–12.07 Å^{-1}).

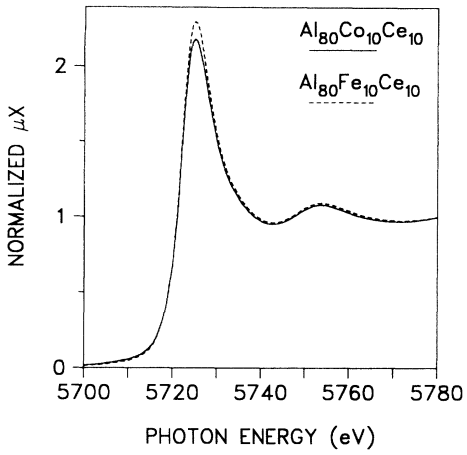

FIG. 9. Comparison of normalized Ce L_3-edge XANES data for 3-μm-thick films of $Al_{80}Co_{10}Ce_{10}$ and $Al_{80}Fe_{10}Ce_{10}$. The XANES displays a highly prominent white line arising from transitions to localized empty d states near the Fermi level.

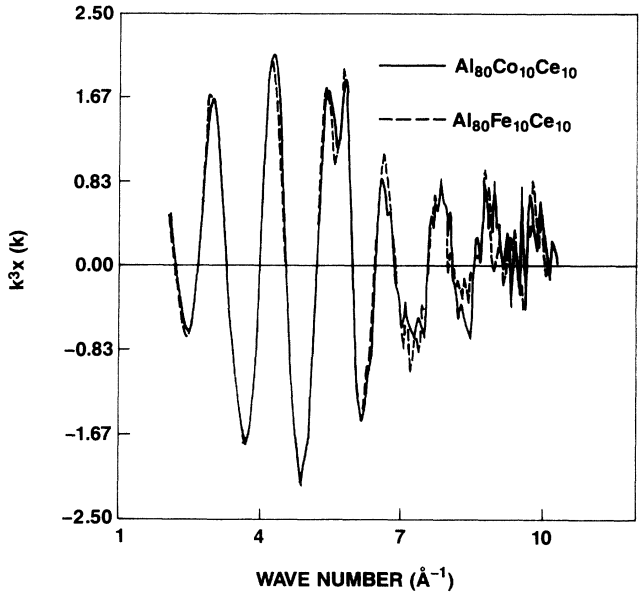

FIG. 10. Comparison of normalized Ce L_3-edge EXAFS data, $k^3\chi(k)$, for 3-μm-thick films of $Al_{80}Co_{10}Ce_{10}$ and $Al_{84}Co_8Ce_8$.

form of Co K-edge data relative to that of Fe K-edge data is mainly due to a smaller disorder in the local structure of Co relative to that of Fe.

The normalized XANES of the Ce L_3 edge for the 3-μm-thick films of $Al_{80}Co_{10}Ce_{10}$ and $Al_{80}Fe_{10}Ce_{10}$ are shown in Fig. 9. Both spectra display prominent white line due to enhanced absorption associated with transitions to well localized empty d states near the Fermi level. In addition, it is also observed that the intensity and the area of the white line for the Fe system are somewhat larger than those of the Co system. It has been shown that the area under the white line after subtraction of an appropriate background can be related to the number density of unoccupied states near the Fermi level.[19] Thus, the increase in the area of the white line for the Fe system relative to that of the Co system indicates that the electron density on the Ce atoms is greater in the Co system from that in the Fe system.

The Ce L_3-edge, $k^3\chi(k)$ spectra, for the three 1-μm-thick films of $Al_{100-2x}Co_xCe_x$ ($x=8,9,10$) and that of the 3-μm-thick film of $Al_{80}Co_{10}Ce_{10}$ are very similar. Hence, only the normalized Ce L_3-edge $\chi(k)$ spectrum for the 3-μm-thick film of $Al_{80}Co_{10}Ce_{10}$ is compared in Fig. 10 with that of the 3-μm-thick film of $Al_{80}Fe_{10}Ce_{10}$. The $k^3\chi(k)$ spectra shown in Fig. 10 were taken in the transmission mode. Their respective Fourier transforms are shown in Fig. 11. Examination of the spectra in Figs. 10 and 11 reveals that in the vicinity of Ce the local structure in both alloys is very similar. One striking feature displayed by the Fourier transforms of Fig. 11 is the presence of up to three well-defined coordination spheres. This is indicative of a structure which is somewhat ordered in the vicinity of Ce in contrast to that observed in the vicinity of Co or Fe.

Quantitative analysis to obtain bond lengths, coordination numbers, and disorders of the first coordination sphere were made as follows. The contribution of the first coordination sphere to $\chi(k)$ is obtained by filtering and back transforming over an r-space range of $\Delta r=0.66-2.78$ Å for Co, 0.82–2.62 Å for Fe, and 1.20–3.30 Å for Ce to allow quantitative analysis of k-space amplitudes and phases using standard procedures. The Δr values were chosen to include the contribution from the first coordination sphere and portions of one loop to the left and another to the right side of the main

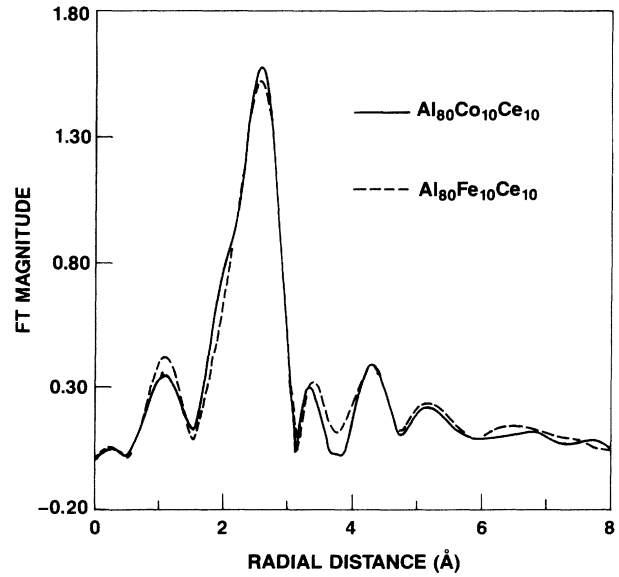

FIG. 11. Comparison of Fourier transforms of normalized Ce L_3-edge EXAFS data, $k^3\chi(k)$, for 3-μm-thick films of $Al_{80}Co_{10}Ce_{10}$ and $Al_{80}Fe_{10}Ce_{10}$ (Δk: 2.17–9.13 $Å^{-1}$).

peak. The filtered EXAFS data is related to the structural parameters by the formula

$$\chi(k)=-\sum_i C_i(k)\sin[2kR_i+2\delta(k)+\phi_i(k)] , \quad (5)$$

where the index i denotes a specific type of atom located at an average distance R_i from the central absorbing atom. The terms $\delta(k)$ and $\phi(k)$ represent the modification in the phase shift of the ejected photoelectron wave function by the potential of the central absorbing and backscattering atoms, respectively. The amplitude term $C_i(k)$ is given by

$$C_i(k)=\frac{N_i}{kR_i^2}S_0^2A(k)F_i(\pi,k,R)e^{-2[R_i/\lambda(k)]}e^{-2\sigma_i^2k^2} , \quad (6)$$

where N_i is the number of atoms of the ith type at distance R_i. The term σ_i is the disorder or root-mean-square deviation about the average distance R_i which includes both a dynamic term arising from thermal motion of the atoms and a static term describing structural disorder. The other terms $\lambda(k)$, $F_i(\pi,k,R)$, and $A(k)$ represent the electron mean free path, the magnitude of the effective curved-wave backscattering amplitude for the ith type of atom, and central atom losses, respectively. Finally, S_0^2 is an energy-independent many-body amplitude reduction factor which accounts for losses only within the central absorbing atom.[17,18] The S_0^2 factor for a particular type of central absorbing atom is a global constant which is shell independent and its magnitude does not depend on the chemical nature and type of backscattering atoms or details of the local structure. The magnitude of S_0^2 is determined from XAFS data of reference compounds with known structure to permit accurate determination of coordination numbers for samples with unknown structure as will be described later in the text.

In fitting the filtered EXAFS spectra with Eq. (5), four parameters per shell are usually varied: coordination number (N), coordination distance (R), disorder squared (σ^2), and an inner potential energy shift (ΔE_0) used in the final definition of the photoelectron wave number $\mathbf{k}$. Since the information content of the EXAFS data is bandwidth limited, the maximum number of fit parameters must not exceed the number of independent data points $N_{\rm pts}$ given by the formula, $N_{\rm pts}=2\Delta k\Delta R/\pi$, where Δk is the k-space range over which $\chi(k)$ is fitted and ΔR is the filtered R-space range of the Fourier transform.[20,21] In our investigation, fits for both Co and Fe for the alloys were done in the k range of 3.0–11.0 Å^{-1}, while fits for Ce were made in the range of 3.0–9.0 Å^{-1}. The fit ranges were chosen in such a way to exclude small portions at the beginning and end of the filtered data range which may have been altered due to the finite range of the inverse Fourier transformation process. Hence, a Δk of 8.0 Å^{-1} for both Co and Fe, a ΔR of 2.12 Å for Co and 1.8 Å for Fe, a Δk of 6.0 Å^{-1} and a ΔR of 2.1 Å for the Ce were used. Thus, the maximum number of parameters that can be varied is ten for Co, nine for Fe-edge data, and eight for the Ce L_3-edge data. In practice, it is customary to choose ΔR values that are significantly larger than the width of the Fourier transform peak in order to minimize truncation errors introduced by the finite range of the integration used in the back-transformation process. This was the case here and, hence, $N_{\rm pts}$ values quoted above are overestimated. The appropriate values of ΔR that must be used in estimating $N_{\rm pts}$ are 1.5 Å for both Co and Fe edge data and 1.7 Å for Ce edge data. Thus, the revised $N_{\rm pts}$ values are eight for both the Co and Fe data and six for the Ce data.

In fitting the filtered data for the reference compounds namely, metallic Fe foil, metallic Co foil, and $Ce(NO_3)_3$ we have constrained the coordination number N to the crystalline value and varied S_0^2, R, σ^2, and ΔE_0. The only exception is in analyzing the first peak in the Fourier transform of Fe metal with bcc lattice which consists of XAFS contributions from two coordination spheres. Hence, a two-shell fit is required and, thus, N_1 and N_2 were constrained to the crystalline values of 8 and 6, respectively, and six parameters (S_0^2, R_1, R_2, σ_1^2, σ_2^2, and ΔE_0) were varied. In all of these fits, *ab initio* theoretical standards based on the curved-wave single scattering formalism were utilized.[17,18] Specifically, the $A(k)$, $\lambda(k)$, $\delta(k)$, $\phi(k)$, and $F(\pi,k,R)$ values were determined using version 3.25 of the FEFF Code.[17,18] In this version, the information required to perform the calculation consists of specifying the type of both the central and backscattering atoms, their bond length ($R_{\rm C\text{-}B}$), the coordination number for the central atom N_C, and the number of central atoms coordinating the backscattering atom N_B. Values of these parameters were obtained from known structural data for the reference compounds Fe,[22] Co,[23] and $Ce(NO_3)_3$ (Ref. 24) and are listed in Table II. The crystal structure for a cerium magnesium nitrate hydrate was used to approximately represent that of cerium nitrate due to lack of its structural data. Results of these numerical fits are listed in Table III. The many-body amplitude reduction factors (S_0^2) were determined to be 0.78 for Fe, 0.75 for Co, and 0.58 for Ce. We have also ana-

TABLE II. Summary of structural data used to generate theoretical standards with the FEFF Code. C-B pair, central-backscattering atoms pair type; $R_{\rm C\text{-}B}$, central-backscattering atoms bond length; N_C, central atom coordination number; N_B, backscattering atom coordination number.

Compound	Fe metal	Al-Fe-Ce	Co metal	Al-Co-Ce	$Ce(NO_3)_3$	Al-Co (or Fe)-Ce
C-B pair	Fe-Fe	Fe-Al	Co-Co	Co-Al	Ce-O	Ce-Al
N_C	8.0	6.0	12.0	6.0	12.0	14.0
N_B	8.0	1.0	12.0	1.0	1.0	1.0
$R_{\rm C\text{-}B}$ (Å)	2.49	2.48	2.51	2.48	2.64	3.25

TABLE III. EXAFS results on reference compounds obtained using theoretical phase and amplitudes calculated with the FEFF code.

Compound	Fit range, Å^{-1}	S_0^2	N[a]	R, Å	δR[b], Å	σ^2, Å^2	ΔE_0, eV
Fe[†]	3.0–17.0	0.782(0.007)	8.0	2.473	−0.010	0.00440	−3.6
			6.0	2.852	−0.015	0.00613	
Co	2.5–16.8	0.746(0.012)	12.0	2.496	−0.013	0.00612	−4.0
	4.0–16.8	0.746(0.012)	12.0	2.496	−0.013	0.00612	−4.0
$Ce(NO_3)_3$	2.0–09.0	0.566(0.021)	12.0	2.590	NA	0.01054	−3.3
	3.0–09.0	0.586(0.026)	12.0	2.596	NA	0.01104	−3.8
	2.0–10.0	0.587(0.023)	12.0	2.585	NA	0.01143	−3.0

[a]Coordination numbers were constrained to crystallographically known values to allow accurate determination of S_0^2.

[b]$\delta R = R$ (fit) $- R$ (crystallography). It shows that distances obtained with theoretical standards are slightly smaller than the known crystallographic distances. NA, not available due to lack of structural parameters for $Ce(NO_3)_3$.

[†]The first peak in the Fourier transform of metallic Fe with bcc lattice contain contributions from the first and second coordination spheres. Hence, a two-shell fit is required to analyze this set of data. In this fit, the many-body amplitude reduction factor (S_0^2) and the inner potential parameter (ΔE_0) were constrained to be same for both shells.

lyzed the XAFS data of Fe_2O_3 and CeO_2 and obtained values for S_0^2 that are consistent with those of metallic Fe and cerium nitrate, respectively. Examination of data listed in Table III shows the reliability of our procedure by virtue of (i) accurate distance determination as indicated by the small values of δR and (ii) disorders that are consistent with theoretical estimates for metallic Fe.[25]

Single-shell fits were sufficient to satisfactorily model the filtered XAFS spectra of Co and Fe in the alloys. Consequently, four floating parameters (which is less than the maximum number of allowable fit variables given by the N_{pts} formula as discussed above) were employed in each fit. Single-shell fits employed for the analysis of the Ce local structure yielded extremely high disorders which can only be resolved by applying a two-shell fit (see Table IV). Single-shell analyses were made with S_0^2 being constrained to values determined from the reference compounds and varying N, R, σ^2, and ΔE_0.

TABLE IV. Summary of EXAFS determined local structure parameters for Co, Fe, and Ce in aluminum-rich amorphous alloys. The "*F*" and "*T*" in parentheses following the sample composition refer to analysis made from XAFS spectra measured in the fluorescence mode and transmission mode, respectively. The data for the Ce-Al C-B pair corresponds to results from the single-shell fit, while the for the Ce-Al(1) and Ce-Al(2) C-B pairs corresponds to the results obtained from the two-shell fit. In the two-shell fit the following constraints were made: $\sigma_1^2 = \sigma_2^2$ and $\Delta E_{01} = \Delta E_{02}$. Error bars were estimated by calculating the standard deviation of several results obtained from various scans and/or by varying various options of the analysis procedure such as the k range of the fit. N, Coordination number; R, Coordination distance. Distances corrected for a small contraction namely, $\delta R = -0.013$, which is mainly an artifact of the use of theoretical standards are included in parentheses (see Table III for more details). σ^2, Mean-square relative displacement in R; ΔE_0, Inner potential used in the final definition of the photoelectron wave number.

Composition	C-B Pair	N	R, Å	σ^2, Å^2	ΔE_0, eV
$Al_{80}Co_{10}Ce_{10}$ (F)	Co-Al	5.8±0.2	2.423(2.44±0.01)	0.0099±0.0003	0.2±0.2
1-μm-thick films					
$Al_{82}Co_9Ce_9$ (F)	Co-Al	6.2±0.2	2.424(2.44±0.01)	0.0096±0.0003	−0.1±0.2
1-μm-thick films					
$Al_{84}Co_8Ce_8$ (F)	Co-Al	6.4±0.2	2.421(2.44±0.01)	0.0090±0.0003	−0.2±0.2
1-μm-thick films					
$Al_{80}Co_{10}Ce_{10}$ (T)	Co-Al	5.9±0.2	2.420(2.44±0.01)	0.0095±0.0003	0.3±0.8
3-μm-thick films	Ce-Al	13.2±0.8	3.112(3.13±0.01)	0.0239±0.0008	2.2±0.3
	Ce-Al(1)	4.4±0.4	2.932(2.95±0.01)	0.0120±0.0008	4.8±0.2
	Ce-Al(2)	8.8±0.2	3.132(3.15±0.01)	0.0120±0.0008	4.8±0.2
$Al_{80}Fe_{10}Ce_{10}$ (T)	Fe-Al	6.4±0.2	2.456(2.47±0.01)	0.0112±0.0003	1.8±0.1
3-μm-thick films	Ce-Al	13.7±1.3	3.093(3.11±0.01)	0.0218±0.0011	2.4±0.4
	Ce-Al(1)	4.6±0.5	2.931(2.94±0.01)	0.0100±0.0021	4.5±1.0
	Ce-Al(2)	8.3±0.8	3.122(3.14±0.02)	0.0100±0.0021	4.5±1.0

The Ce two-shell analysis was made with S_0^2 being constrained to the value determined from the reference and varying N_1, N_2, R_1, R_2, σ_1^2, and ΔE_0 with σ_2^2 being constrained to equal σ_1^2. Again, these fits were performed with theoretical standards calculated with the FEFF code (version 3.25) using structural data listed in Table II. Three different sets of theoretical standards were generated allowing for a 0, 10, and 20% overlapping atomic potentials. Fits were performed with each set of theoretical standards using both no-weighted and k^3-weighted filtered data. For both the Fe and Co K-edge EXAFS fits, theoretical standards calculated with 10% overlapping potentials produced significantly better fits in the low k region as revealed from fits made to the no-weighted filtered data. In, addition, numerical results from fits to the data with no k-weighting were also similar to those obtained from fitting the k^3-weighted data. Theoretical standards calculated for the Ce-Al chemistry with no overlapping were sufficient to fit the Ce L_3-edge filtered EXAFS data. Results of these numerical fits are listed in Table IV. Typical comparisons of filtered and calculated EXAFS spectra for the Co K-edge and Ce L_3-edge EXAFS spectra for $Al_{84}Co_8Ce_8$ are shown in Figs. 12 and 13.

As described previously, the analysis of filtered EXAFS spectra was carried out employing a Gaussian disorder which is only suitable for truly Gaussian pair-distribution functions or in the limit of small disorders. It has been shown that use of symmetric pair-distribution functions to analyze local structures with a high degree of asymmetry leads at least to erroneous distance determination. We have analyzed our data using the method of cumulants expansion including up to the fourth term[26] and also using weighted exponential pair-distribution functions.[27] This was done in order to determine if asymmetric pair-distribution functions are more appropriate than the Gaussian distribution function to model the local structure of this class of materials. We have found that no significant improvement in the quality of fits to the experimental data is gained when asymmetric pair-distribution functions are used to model the structure and, hence, the Gaussian disorder represents an appropriate model for the analysis of this material.

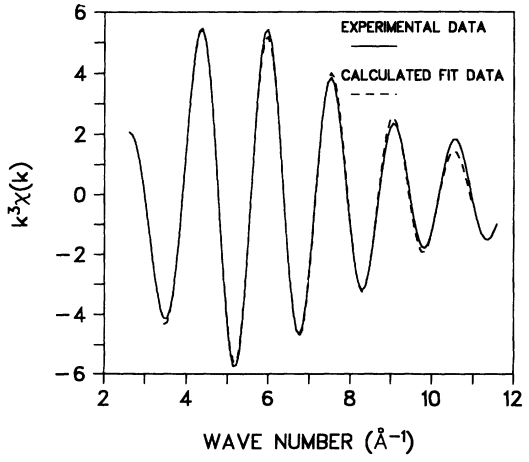

FIG. 12. Comparison of filtered (solid) and calculated single-shell fit (dash) of Co K-edge EXAFS data using structural data listed in Table IV for $Al_{84}Co_8Ce_8$. Fit range of 3.0–11.0 Å^{-1} and k^3-weighted data.

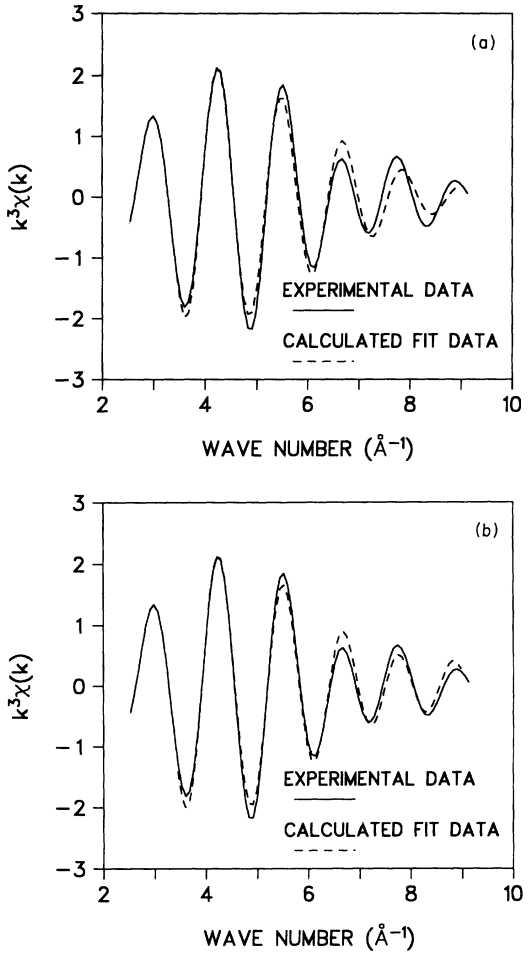

FIG. 13. (a) Comparison of filtered (solid) and calculated single-shell fit (dash) of Ce L_3-edge EXAFS data using structural data listed in Table IV for $Al_{84}Co_8Ce_8$. Fit range of 3.0–9.0 Å^{-1} and k^3-weighted data. (b) Comparison of filtered (solid) and calculated two-shell fit (dash) of Ce L_3-edge EXAFS data using structural data listed in Table IV for $Al_{84}Co_8Ce_8$. Fit range of 3.0–9.0 Å^{-1} and k^3-weighted data.

DISCUSSION

Our results, summarized in Table IV, show that the first coordination sphere of cobalt consists of 5.8 to 6.4 aluminum atoms at a distance of 2.44 Å. The coordination number appears to increase slightly, while disorder decreases slightly with increase in Al content within the composition range investigated. The Co-Al distance remains constant independent of composition. The first coordination sphere of Fe consists of 6.4 Al atoms at a distance of 2.47 Å, which is slightly longer than that of Co-Al. Single-shell fits of the Ce local structure indicate that Ce is coordinated with roughly 14 Al atoms at a distance of 3.13 Å in the Al-Co-Ce system and 3.11 Å in the

Al-Fe-Ce system. Disorders obtained from single-shell fits of both systems for Ce-Al coordination, however, are extremely large indicating a high degree of structural disorder. The high degree of structural disorder indicates a distribution of Ce-Al distances within the first coordination sphere. The fact that the Fourier transforms of Ce L_3-edge EXAFS spectra display well-defined peaks corresponding to second and third coordination spheres indicates that the distribution of these distances must correspond to a small number of subshell distances. In fact, the large degree of structural disorder based on single-shell-fit results for Ce, can be resolved assuming that the first coordination sphere of Ce contains two subshells of Ce-Al coordination. This is demonstrated by the results from the two-shell fit. These results reveal that Ce in both systems is coordinated with roughly five Al atoms at a distance of 2.95 Å and nine Al atoms at a distance of 3.15 Å. The sum of the coordination numbers obtained from the two-shell fit is consistent with the single-shell fit coordination number. The weighted average distances calculated from the two-shell fit results are 3.08 and 3.07 Å for $Al_{80}Co_{10}Ce_{10}$ and $Al_{80}Fe_{10}Ce_{10}$, respectively. The disorders obtained from the two-shell fit are much smaller than those of the single-shell fit disorders and compare favorably with disorders of the Co-Al and Fe-Al environments.

A comparison of EXAFS determined Fe and Ce local structures of the magnetron-sputtered amorphous alloys of this investigation with the results from a pulsed neutron and x-ray-scattering experiments and diffraction using synchrotron radiation made on liquid-quenched amorphous ribbons of composition $Al_{90}Fe_xCe_{10-x}$ ($x=3,5,7$) by Hsieh and co-workers[8,9] will now be made. Our results for the magnetron-sputtered amorphous $Al_{80}Fe_{10}Ce_{10}$ alloy show an Fe coordination which is similar to that obtained by Hsieh and co-workers who conclude that the Fe coordination for liquid-quenched amorphous $Al_{90}Fe_5Ce_5$ and $Al_{90}Fe_7Ce_3$ consists of 6.2 and 6.3 Al atoms at a distance of 2.49 Å, respectively. Hsieh and co-workers also concluded that the second coordination sphere of Fe consists of 3.8 Al atoms at a distance of approximately 2.8 Å. However, the evidence for the presence of the second shell of atoms is indirect and we believe that it is somewhat uncertain. The contribution of this second coordination sphere is absent from the Fourier transforms of the EXAFS spectra of magnetron-sputtered alloys and hence cannot be investigated. Its absence may be due to a high degree of structural disorder associated with this shell of atoms. The EXAFS determined Ce local structure of magnetron-sputtered amorphous $Al_{80}Fe_{10}Ce_{10}$ alloy differs significantly from that of liquid-quenched amorphous $Al_{90}Fe_xCe_{10-x}$ ($x=3,5,7$) alloys as determined by Hsieh *et al.*[9] Our results reveal that two Ce-Al distances contribute to the Ce-Al correlation in contrast to only the single distance predicted by x-ray-scattering and diffraction experiments. Namely, EXAFS shows a Ce coordination consisting of roughly five and nine Al atoms at distances of 2.95 and 3.15 Å, respectively, compared to 14 ± 1.6 and 11.0 ± 2.3 Al atoms for liquid-quenched $Al_{90}Fe_5Ce_5$ and $Al_{90}Fe_7Ce_3$, respectively, at a distance of 3.25 Å. While the sum of the coordination numbers for magnetron-sputtered alloys is in agreement with the coordination number for liquid-quenched alloys, the distances are significantly shorter. The observation of a split shell of atoms by the EXAFS method in contrast to a single shell of atoms by the neutron method is not surprising if one considers the atomic specificity of the EXAFS method which allows measurements of the radial structure function for each of Al, Fe, and Ce separately. The EXAFS measured radial structure function for Ce is not complicated by contributions from the radial structure functions of Al and Fe and hence more information can be extracted with regard to the local structure of Ce. The neutron-scattering experiments measures the total pair-distribution function of the system which includes contributions from the Fe-Al, Fe-Fe, Fe-Ce, Ce-Al, Ce-Ce, and Al-Al correlations. Admittedly, contributions from the Fe-Fe, Fe-Ce, and Ce-Ce are very small and can be ignored. However, contributions from the remaining correlations are strong and can overlap with each other making extraction of detailed structural information more difficult from neutron-scattering data than from EXAFS data.

Based on the dense random packing (DRP) model of hard spheres,[13] using the principle of two-dimensional packing, the coordination number can be estimated using the following two equations:

$$\omega_{BA}=2\pi\left[1-\frac{\sqrt{R_B(R_B+2R_A)}}{R_A+R_B}\right] \tag{7}$$

and

$$N_{BA}=4\pi\frac{\eta_{II}}{\omega_{BA}}\ , \tag{8}$$

where ω_{BA} is the solid angle subtended by A atom at B atom, $R_{A(B)}$ is the atomic radius of $A(B)$ atoms, N_{BA} number of A atoms coordinating the B atoms, η_{II} is the two-dimensional packing density ($=0.842$ for dense random packing). Using Eqs. (7) and (8) employing the metallic state atomic radii of Co, Fe, Ce, and Al, it is estimated that $N_{\text{Co-Al}}=11$, $N_{\text{Fe-Al}}=11$, and $N_{\text{Ce-Al}}=16$. The corresponding A-B pair distances based on this model calculated using the formula $R_{A\text{-}B}=R_A+R_B$ are estimated to be $R_{\text{Co-}Al}=2.68$ Å, $N_{\text{Fe-}Al}=2.69$ Å, and $N_{\text{Ce-Al}}=3.25$ Å.

Thus, our EXAFS determined distance for the Co-Al pair is smaller than the sum of the atomic radii of Co and Al by 0.24 Å. This corresponds to a 9% contraction in the distance expected on the basis of the DRP model. In addition, the coordination number for Co is also reduced roughly by 45% from that based on the DRP model assuming a coordination of six Al atoms. Similar contraction in coordination distance and reduction in the coordination number are observed for the Fe atoms. These anomalously short distances and low coordination numbers compared to those based on the DRP model indicate that the radii for the Co, Fe, and Al atoms have been significantly altered from those of the metallic state radii

values. The effective radii in the amorphous state can be estimated from the EXAFS determined coordination numbers and distances with the aid of Eqs. (7) and (8) and employing the fact that R_{EXAFS} is equal to the sum of the effective atomic radii. Following this procedure and assuming a Co and Fe coordination of six Al atoms, it is estimated that $R_{eff}(Co)=0.75$ Å and $R_{eff}(Al)=1.69$ Å for the Al-Co-Ce system and $R_{eff}(Fe)=0.75$ Å and $R_{eff}(Al)=1.72$ Å for the Al-Fe-Ce system. The effective atomic radii for Co, Fe, and Al coordinating Co or Fe in the amorphous state are significantly shorter than the corresponding metallic state radii of 1.25, 1.26, and 1.43 Å, respectively. The altered atomic radii of Al, Co, and Fe in the amorphous state indicate a strong interaction between Co or Fe atoms and the Al atoms, perhaps as a result of a covalently bonded environment. The dramatically reduced radius for Fe and increased radius for Al have been attributed to be due to the transfer of electrons with *s-p* character of the Al atoms to the *d* states of the Fe atoms.[8] This hypothesis is consistent with conclusions made on the basis of the XANES spectra which indicate a charge transfer from the Al atoms to neighboring Fe atoms. It has been shown by Kabacoff *et al.*[3] that the degree of stability of the amorphous Al-Fe-Gd system increases with increase in the Fe content in the composition range similar to that of the Al-Co-Ce and Al-Fe-Ce alloys of the present investigation. The increase in stability of amorphous Al-Fe-Gd with increase in Fe content may be attributed to the strong interaction between the Fe and Al atoms assuming that the strong interaction observed between Fe and Al atoms in the Al-Fe-Ce system is also characteristic of Fe and Al atoms in the Al-Fe-Gd system.

For Ce atoms in both the Al-Co-Ce and Al-Fe-Ce systems, on the other hand, the weighted average Ce-Al distance of 3.08 Å is smaller by 0.17 Å when compared to the sum of the metallic state radii of Al and Ce atoms. This corresponds to a distance contraction of only 5%. The Ce coordination umber of roughly 14 Al atoms is only reduced by 13% from values based on the DRP model. The distance contraction and reduction in the coordination number for Ce atoms are much smaller than those of the Co or Fe atoms. Assuming a coordination number of 14 Al atoms at a weighted average distance of 3.08 and 3.07 Å for Ce in the Co and Fe systems, respectively, the effective atomic radii for Ce and Al coordinating Ce in the amorphous state are estimated to be $R_{eff}(Ce)=1.62$ Å and $R_{eff}(Al)=1.46$ Å for the Al-Co-Ce system and $R_{eff}(Ce)=1.61$ Å and $R_{eff}(Al)=1.46$ Å for the Al-Fe-Ce system. Thus, in the amorphous state, the effective radius for Ce is somewhat shorter, while that of Al is only slightly longer when compared to the metallic state radii of 1.82 and 1.43 Å for Ce and Al, respectively. Hence the local bonding for Ce atoms is likely to be metallic in character.

The effect of the amorphous state radii on the atomic size factor, λ, calculated using Eq. (1), is shown in Table I. It is shown that the composition of the glass-forming region strictly follows the theoretical limit calculated using the amorphous state radii as well as the metallic state radii.

In summary, 1- and 3-μm-thick films of aluminum-rich amorphous alloys of Al-Co-Ce and a 3-μm-thick film of Al-Fe-Ce were prepared using the dc magnetron-sputtering method. These films were initially characterized by x-ray diffraction showing that the structural nature of these films is truly amorphous for samples with composition $Al_{100-2x}Co_xCe_x$ ($x=8$, 9, and 10). Sharp peaks in the x-ray-diffraction patterns characteristic of a crystalline phase or phases were observed for samples with composition $Al_{100-2x}Co_xCe_x$ (where $x \leq 7$). It is shown that the composition of the glass-forming region for magnetron-sputtered alloys strictly follows the theoretical limit based on the atomic size criterion using the metallic state radii or the amorphous state radii. The local atomic structure of Co and Ce in amorphous $Al_{100-2x}Co_xCe_x$ ($x=8$, 9, and 10) and that of Fe and Ce in $Al_{80}Fe_{10}Ce_{10}$ alloys was then investigated by x-ray-absorption fine structure (XAFS) spectroscopy. The following conclusions with regard to local structure of Co, Fe, and Ce are made from analyses of the XAFS spectra. The first coordination sphere of cobalt in $Al_{100-2x}Co_xCe_x$ ($x=8$, 9, and 10) consists of 5.8 to 6.4 Al atoms at a distance of 2.44 Å. The local coordination sphere for Fe in $Al_{80}Fe_{10}Ce_{10}$ consists of 6.4 Al atoms at a distance of 2.47 Å. Ce in both systems is coordinated with roughly five and nine Al atoms at distances of 2.95 and 3.15 Å, respectively. Both Co-Al and Fe-Al bond lengths are anomalously short with also anomalously low coordination numbers from values expected on the basis of the DRP model using the metallic state radii. The distance contraction and reduction in the coordination number for Ce are much smaller than those of Co or Fe. The anomalous changes for Co and Fe in the amorphous state indicate a strong interaction between Co or Fe atoms and the Al atoms which perhaps may be a result of a covalently bonded environment. Local bonding for Ce, on the other hand, is likely to be metallic in character.

ACKNOWLEDGMENTS

This work was supported by the Independent Research (IR) Program of the Naval Surface Warfare Center. We also acknowledge the support of the U.S. Department of Energy, Division of Materials Sciences, under Contract No. DE-AS05-80-ER10742 for its role in the development and operation of Beam Line X-11 at the National Synchrotron Light Source (NSLS). The NSLS is supported by the Department of Energy, Division of Materials Sciences and Division of Chemical Sciences, under Contract No. DE-AC02-76CH00016.

*Author to whom all correspondence should be sent: Naval Surface Warfare Center, Dahlgren Division, Detachment White Oak, Code R34, Bldg. 30-213, 10901 New Hampshire Avenue, Silver Spring, MD 20903-5000.

[1]Y. He, S. J. Poon, and G. J. Shiflet, Science **241**, 1640 (1988).

[2]A.-P. Tsai, A. Inoue, and T. Masumoto, Metall. Trans. A **19A**, 1369 (1988).

[3]L. T. Kabacoff, C.-P. Wong, N. L. Guthrie, and S. Dallek, Mater. Sci. Eng. A **134**, 1288 (1991).

[4]G. J. Shiflet, Y. He, and S. J. Poon, J. Appl. Phys. **64**, 6863 (1988).

[5]A. Inoue, K. Ohtera, and A.-P. Tsai, Jpn. J. Appl. Phys. **27**, 938 (1988); **27**, L479 (1988).

[6]J. L. Wagner, K. M. Wong, F. S. Pierce, and S. J. Poon, Phys. Rev. B **39**, 5500 (1989).

[7]T. Egami and Y. Waseda, J. Non-Cryst. Solids **64**, 113 (1984).

[8]H. Y. Hsieh, B. H. Toby, T. Egami, Y. He, S. J. Poon, and G. J. Shiflet, J. Mater. Res. **5**, 2807 (1990).

[9]H. Y. Hsieh, T. Egami, Y. He, S. J. Poon, and G. J. Shiflet, J. Non-Cryst. Solids **135**, 248 (1991).

[10]D. E. Sayers, S. M. Heald, M. A. Pick, J. I. Budnick, E. A. Stern, and J. Wong, Nucl. Instrum. Methods Phys. Res. **208**, 631 (1983).

[11]J. Jaklevic, J. A. Kirby, M. P. Klein, A. S. Robertson, G. S. Brown, and P. Eisenberger, Solid State Commun. **23**, 679 (1977).

[12]F. W. Lytle, R. B. Greegor, D. R. Sandstrom, E. C. Marques, J. Wong, C. L. Spiro, G. P. Huffman, and F. E. Huggins, Nucl. Instrum. Methods Phys. Res. Sec. A **226**, 542 (1984).

[13]T. Egami and V. Vitek, in *Amorphous Materials: Modeling of Structure and Properties,* edited by V. Vitek (TMS-AIME, Warrendale, 1983), p. 127.

[14]W. H. McMaster, N. Kerr Del Grande, J. H. Mallet, and J. H. Hubbell, *Compilation of X-ray Cross Sections* (National Technical Information Service, Springfield, VA, 1969).

[15]D. E. Sayers and B. A. Bunker, in *X-Ray Absorption, Principles, Applications, Techniques of EXAFS, SEXAFS and XANES,* edited by D. C. Koningsberger and R. Prins (Wiley, New York, 1988), p. 211.

[16]J. W. Cook, Jr., and D. E. Sayers, J. Appl. Phys. **52**, 5024 (1981).

[17]J. J. Rehr, J. Mustre de Leon, S. I. Zabinsky, and R. C. Albers, J. Am. Chem. Soc. **113**, 5136 (1991).

[18]J. Mustre de Leon, J. J. Rehr, and S. I. Zabinsky, Phys. Rev. B **44**, 4146 (1991).

[19]A. N. Mansour, J. W. Cook, and D. E. Sayers, J. Phys. Chem. **88**, 2330 (1984).

[20]F. W. Lytle, D. E. Sayers, and E. A. Stern, Physica B **158**, 701 (1989).

[21]*X-Ray Absorption Fine Structure,* edited by S. S. Hasnain (Horwood, Chichester, UK, 1991), Chap. 195, p. 751.

[22]*Pearson's Handbook of Crystallographic Data for Intermetallic Phases,* edited by P. Villars and L. D. Calvert (American Society for Metals, Metals Park, Ohio, 1985), Vol. 2, p. 1736.

[23]*Pearson's Handbook of Crystallographic Data for Intermetallic Phases* (Ref. 23), Vol. 3, p. 2162.

[24]A. Zalkin, J. D. Forrester, and D. H. Templeton, J. Chem. Phys. **39**, 2881 (1963).

[25]E. Sevillano, H. Meuth, and J. J. Rehr, Phys. Rev. B **20**, 4908 (1979).

[26]G. Bunker, Nucl. Instrum. Methods Phys. Res. **207**, 437 (1983).

[27]M. DeCrescenzi, A. Balzarotti, F. Comin, L. Incoccia, S. Mobilio, and N. Motta, Solid State Commun. **37**, 921 (1981).